

Plasma spray synthesis of nanomaterial powders and deposits

J. Karthikeyan, C.C. Berndt^{*}, J. Tikkanen¹, S. Reddy, H. Herman

The Thermal Spray Laboratory, Department of Materials Science and Engineering, State University of New York at Stony Brook, Stony Brook, NY 11794-2275, USA

Received 6 September 1996; received in revised form 29 October 1996

Abstract

Conventional plasma spraying was used to process atomized liquid droplets of precursor solutions to produce alumina, zirconia and yttria stabilized zirconia nanoparticles and deposits. An electrostatic precipitator collected the plasma synthesized ceramic particles at a rate of -0.2 mg s^{-1} , with -5 – 20% collection efficiency. Spray processing produced 1–50 nm size ceramic particles. The size, shape and phase composition of the nanomaterials depend on the spray feedstock. Organo-metallic precursors gave rise to a narrow range of fine-grained material, while aqueous solutions produced wider distributions of larger size grains. Spray processing of liquid feedstock produced nanodeposits with a powdery morphology. Plasma spraying of liquid precursors is a viable technique to produce nanoparticles and deposits. © 1997 Elsevier Science S.A.

Keywords: Plasma spray; Synthesis; Nanomaterial

1. Introduction

Nanomaterials exhibit unique properties [1–7] that are attractive for various high performance applications. Examples include wear resistant surfaces, low temperature sinterable high strength ceramics, and magnetic nanocomposites. Hence, the synthesis and study of nanomaterials has become an active field, and various techniques have been developed and/or modified to synthesize these materials. These include laser ablation [8], flame processing [9], vapor deposition [10], RF and microwave plasma synthesis [11–13], sol-gel processing [14] and mechanical milling [4]. This article presents a new technique, viz., the Plasma Spray Synthesis (PSS) process, to synthesize nanoparticles and nanodeposits.

Plasma spraying [15] is a mature and advanced materials processing technique. In this process, a high temperature plasma jet is used to melt and spray a feedstock which is injected into the plasma flame. In general, the plasma spray process is used for producing protective and performance enhancing coatings. The

working fluid (plasma flame) has many special characteristics, such as a high enthalpy density, high temperature, high velocity, active environment and extremely high heating and cooling rates. These characteristics can be advantageously used in many novel and special applications [15–17] such as particle spheroidization, reaction synthesis, rapid solidification processing and others. Russian workers have used the plasma reactor systems for manufacturing submicron sized particles by the gas phase synthesis process [18].

The PSS process, reported here, does not use a reaction chamber, but produces nanomaterials by spray pyrolysis in an open atmospheric plasma spray jet. Liquid precursor chemicals are atomized and injected into a plasma jet. Nanoparticles, synthesized by plasma jet spray pyrolysis are collected as powder in an electrostatic precipitator or as a deposit on a substrate. This work has shown that the plasma spray synthesis of nanomaterials has many potential advantages, some of which are listed below.

1. In general, nanomaterials synthesis processes require expensive, complex and specialized equipment, such as ultra-high vacuum systems, high energy mills, high power lasers, etc. The PSS process is a simple industrial process and operates in open atmosphere. Hence, the process should be economical to install and operate.

^{*}Corresponding author. Tel.: +1 516 6328507; fax: +1 516 6328525.

¹ Present address: Tampere University of Technology, Department of Physics, P.O. Box 692, FIN 33101, Tampere, Finland.

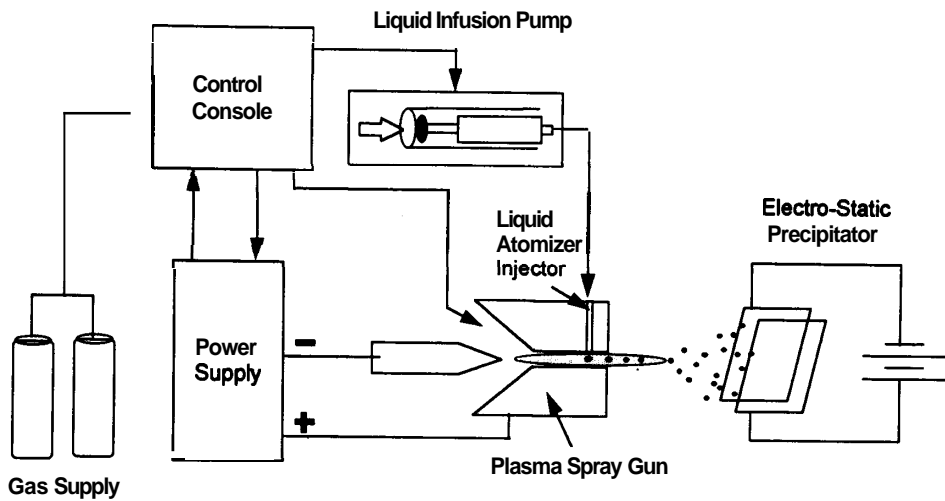


Fig. 1. Schematic of the experimental system.

- The PSS process is highly versatile. Any precursor chemical (nitrates, acetates, oxalates, alkoxides, etc.) and any solvent (water, alcohols and others) can be incorporated into the spray feedstock. Liquid mixtures can be used to produce multicomponent systems such as $ZrO_2-Y_2O_3$, $Y_1Ba_2Cu_3O_7$ and others. Since each droplet contains precursor chemicals in the same stoichiometric composition, as desired in the produced particle, the synthesized particles will have compositional homogeneity.
- PSS has the potential for high through-put processing. With proper design of the spray feedstock injection ports, liquids can be processed in excess of 50 g min^{-1} .
- In a conventional plasma spray process, expensive solid feedstocks are used to produce fine grained ($\sim 0.5-5.0 \mu\text{m}$) deposits. In the PSS process, inexpensive precursor chemicals can be used to obtain nanostructured powders and deposits.

In summary, the PSS combines the simplicity and high through-put of the plasma spray process with versatility and economics of the spray pyrolysis process to produce the desired nanostructured materials.

2. Experiments

2.1. Materials

Alumina, zirconia and 8 wt.% yttria stabilized zirconia (YSZ) were studied in this work since these materials have been well characterized both as sprayed coatings and as nanomaterials [1,5,8–10,14,15]. Aluminum isopropoxide, zirconium butoxide, zirconium acetate and yttrium acetate (Aldrich, Milwaukee, WI) were used as metal organic precursors. Isopropanol, n-butanol and distilled water were used as solvents to

dissolve the precursors and to obtain liquid feedstocks for spray operation. Stainless steel coupons of dimensions $50 \times 25 \times 2 \text{ mm}$ were used as substrates. Ten mesh alumina grit was used to grit blast the substrates prior to spray coating.

2.2. Spray feedstocks

Alumina, zirconia and YSZ feedstocks were prepared as follows. A 1.5 wt.% alumina feedstock was prepared by dissolving 18.03 grams of aluminum isopropoxide in 350 ml of isopropanol at 350 K, under vigorous magnetic stirring. The solution was stirred for a further 30 min at 350 K and then cooled to obtain the alumina feedstock. Similarly, 20 ml of 80 wt.% zirconium butoxide in n-butanol was diluted with 300 ml of n-butanol to obtain the 2.4 wt.% zirconia feedstock. Yttrium acetate (12.34 g) was dissolved in 1000 g of zirconium acetate in dilute acetic acid under constant magnetic stirring. This solution was further diluted with 520 ml of distilled water to obtain 2 wt.% YSZ feedstock.

2.3. Experimental system

Figure 1 presents a schematic of the experimental system in the configuration used for collecting the powder. The electrostatic precipitator is replaced by the substrate for producing the deposits. Powder and deposit specimens were collected with each set of experimental conditions. A standard infusion pump (Harvard Apparatus, MA, USA) was used to deliver the liquid feedstock to the liquid atomizer injector. This injector (Fig. 2), which works on the two-fluid atomization principle, produces atomized droplets of the feedstock and injects it into the high pressure plume of the plasma jet. A conventional atmospheric plasma spray torch (Miller Thermal SG 100), whose powder injection

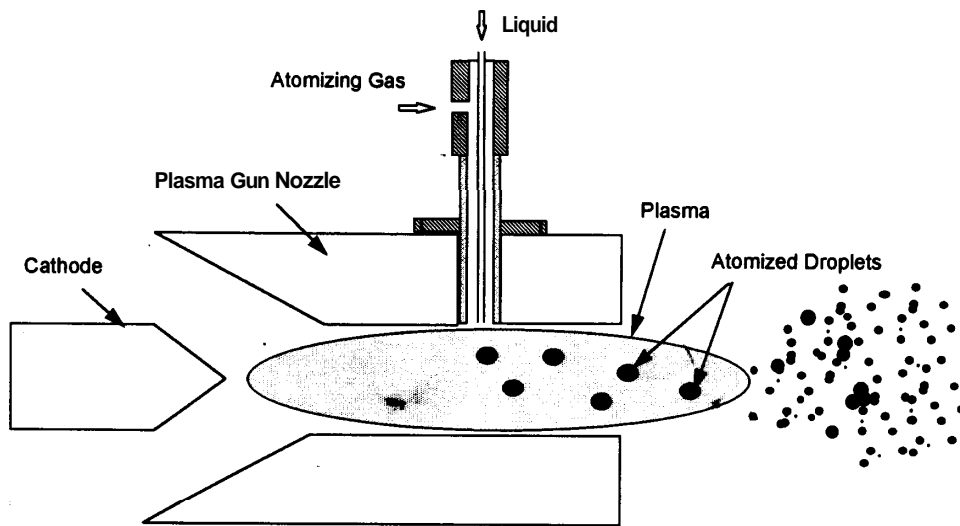


Fig. 2. Schematic of the liquid atomizer injector.

port and tube have been modified to incorporate the injector, was used to produce the high temperature plasma flame. A parallel plate electrostatic precipitator, which consists of a pair of polished 100 x 100 x 2 mm stainless steel plates separated by a 10 mm thick ceramic insulator, is placed parallel to the trajectory of the spray beam. An electric field of 6 kV cm^{-1} was applied in the electrostatic precipitator so that the spray particles could be collected on the plates by electrophoresis. For producing the coatings, the electrostatic precipitator is replaced by the grit blasted substrate and the spray gun is scanned over the substrate surface.

2.4. Specimen preparation and characterization

Spray synthesis of nanomaterials with consistent characteristics requires control of the size and size distribution of atomized liquid droplets and optimization of the spray parameters. Hence, a series of experiments was carried out by varying the diameter of the atomizing nozzle, the pressure and flow rate of the atomizing gas and the concentration and flow rate of the liquid feedstock, and recording the variations in the droplet size distribution of the aerosols using a laser scattering technique (J. Tikkanen, J. Karthikeyan, V. Pitkanen, K.A. Gross, S. Raghu, G. Graeffe, C.C. Berndt (unpublished research)). A typical result of this study, obtained by the laser scattering technique, is shown in Fig. 3, which shows the droplet size variation with respect to the flow rate of atomizing gas. Based on the results of these experiments, atomization and spray parameters were optimized, and these parameters are given in Table 1. All subsequent specimens were prepared using these parameters only.

Microstructural features of the specimens were studied using the scanning electron microscopy (SEM-Model JSM 5300, Jeol). Specimen shape, size and texture were studied in both secondary electron image and back scattered electron image modes. An XRD (Model PW 1729, Philips) was used to establish the phase composition of the specimen.

The collected powder was dispersed ultrasonically in alcohol and then allowed to settle on carbon coated copper grids for investigation by transmission electron microscopy (TEM-Model CM 12, Philips) attached with an energy dispersive analysis of X-ray (EDAX) facility. Bright field and dark field images were used to study the particle size and texture, while selected area diffraction (SAD) was used to study the specimen granularity. The specimen chemistry was established by the EDAX.

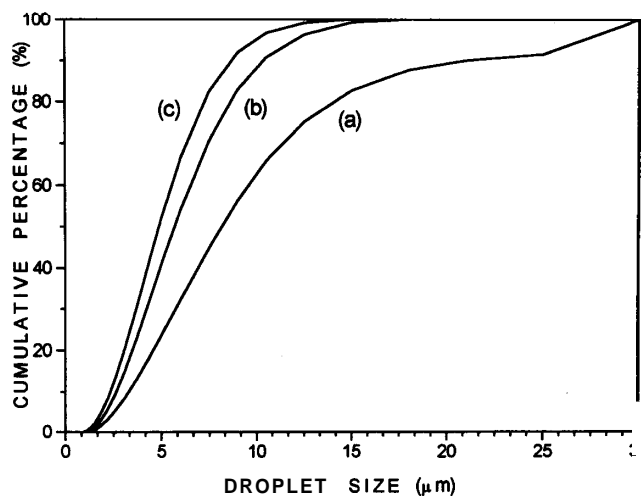


Fig. 3. Size distribution of atomized droplet at (a) 6 LPM, (b) 8 LPM and (c) 10 LPM of atomizing gas flow rates.

Table 1
Optimized process parameters

No.	Parameter	Optimized value
1	Liquid feed rate (ml min ⁻¹)	5.0
2	Atomizing gas pressure (kg cm ²)	9.0
3	Atomizing gas flow rate (SLPM)	10.0
4	Plasma gas 1 (Ar) flow rate (SLPM)	50
5	Plasma gas 2 (H ₂) flow rate (SLPM)	0.7
6	Arc current (A)	600
7	Arc voltage (V)	50
8	Stand off distance (mm)	100
9	Diameter of the atomizer liquid nozzle (mm)	0.8
10	Diameter of the atomizing gas nozzle (mm)	1.2

XRD peak width analysis was carried out to estimate the particle size [20–22]. The diffraction pattern of the specimen was recorded at a speed of 0.01° s⁻¹ using Cu K α radiation with a nickel filter, and the full width at half-maxima (FWHM) of the diffraction peaks was measured. Contributions due to K α_1 and K α_2 were deconvoluted, and only the K α peak widths were taken for calculation. XRD of a standard silica specimen was used to measure instrument broadening, and Ziegler's [21] method was used to remove the instrument broadening for obtaining the true crystal broadening of the specimen. Using the Scherrer relationship for size effect and Cauchy's correction for stress effects, the following relationship is obtained.

$$\beta \cos \theta = K\lambda/D + 4\Delta d/d \sin \theta \quad (1)$$

where β is the corrected true FWHM of the diffraction peak, θ is the diffraction angle, K is the shape constant (close to unity), λ is the wave length of the radiation, D is the size of the crystallite, Δd is the lattice strain and d is the lattice dimension. The parameter $\beta \cos \theta$ was plotted vs. $\sin \theta$, and as shown by Eq. (1), a straight line is obtained with the intercept given by the crystal size and the slope revealing the stress effect. However, it should be noted that in this experimental technique the correction procedure and deconvolution process strongly affect [20,21] the estimated grain size, and hence the XRD estimated particle size should be treated only as an order of magnitude value.

3. Results

Experiments showed that plasma synthesis of ultrafine particles and their collection in the electrostatic precipitator can be achieved typically at a rate of around 0.2 mg s⁻¹ with about 5–20% collection efficiency. Thick film deposits, similar to the solid particle deposits reported by Gurav et al. [23], were obtained at a deposition rate of around 3–5 $\mu\text{m min}^{-1}$. The depo-

sition efficiencies of the coatings were less than 10.0%. The coatings exhibited a powdery structure with poor adhesive and cohesive strengths, requiring high temperature heat treatment for densification of the deposit [24].

3.1. Alumina

Topographical features of a typical specimen are shown in Fig. 4. The deposit is discontinuous, and the substrate is visible at some locations. The specimen presents a powdery structure, and at high magnifications 10–50 nm size particles can be distinguished. These particles have aggregated into large (micron sized) irregular shaped blocks, which are loosely bound onto the substrate as well as to other aggregates.

The XRD of a typical deposit and powder specimens are presented in Fig. 5. They show that the powder consists of γ alumina while the deposit is made of δ alumina. The deposit XRD also contains the diffraction peaks of the substrate material, since the deposit is discontinuous. During the deposition process, the substrate had been overheated by the plasma flame, leading

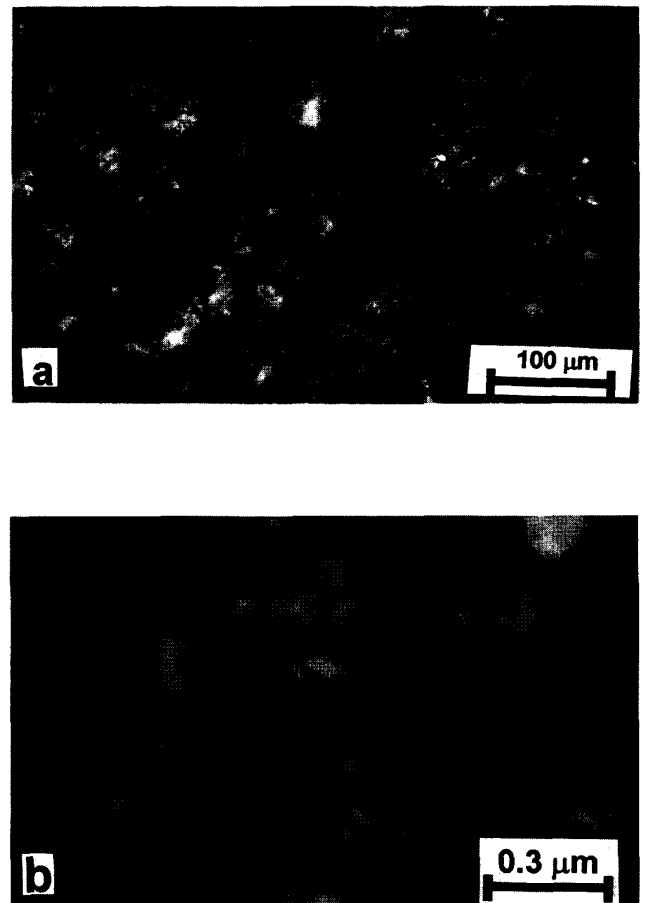


Fig. 4. Microstructures of a typical alumina deposit at (a) low and (b) high magnifications.

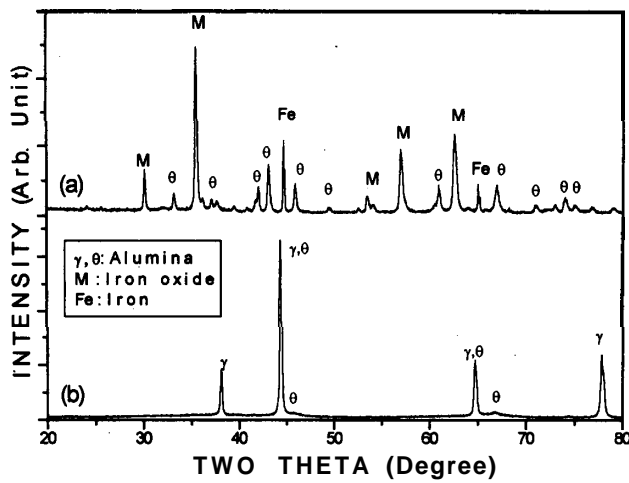


Fig. 5. XRD of alumina specimens (a) deposit and (b) powder.

to oxidation. This resulted in the formation of magnetite on the substrate surface. Table 2 gives the size of the γ and θ alumina phases calculated using the Scherrer-Cauchy relationship (Eq. (1)).

A typical TEM image of the powder is presented in Fig. 6, which shows that the specimen consists of nanometer-sized particles, confirming that the crystal sizes measured by the XRD represent only an order-of-magnitude value. The micrograph shows that many of the nanoparticles have formed large aggregates. Dark field studies showed that the individual particles in the aggregates are single crystals of $\sim 2-5$ nm dimensions. The selected area diffraction of these particles (inset in Fig. 6) presents many discrete rings, showing that the diffraction area consists of a large number of ultrafine crystalline powder particles.

3.2. Zirconia

Zirconia deposits show a powdery structure, Fig. 7. As compared to alumina, this deposit contains fewer voids and almost completely covers the surface of the substrate. Similar to the alumina deposit, the zirconia deposit also consists of 20-80 nm size particles, which

Table 2
Scherrer-cauchy crystallite sizes

Material	Phase	Crystal size (nm)	
		Deposit	Powder
Alumina	Gamma (γ)	—	96
	Theta (θ)	499	—
Zirconia	Tetragonal	25	36
	Monoclinic	86	77
YSZ	Tetragonal	55	39
	Monoclinic	85	95

have agglomerated into micrometer-sized particles. There is an apparent lack of cohesion between the individual particles within the agglomerates and between different agglomerates. Fig. 8 presents the XRD of typical powder and deposit specimens. It shows that the zirconium butoxide feedstock has been completely transformed into tetragonal (t) and monoclinic (m) zirconia. The relative weight percentage of the tetragonal and monoclinic phases vary between the powder and deposit specimens. The XRD of the deposit contains the iron and iron oxide peaks, showing that this deposit is discontinuous and that the substrate has been oxidized during the spray process. The Scherrer analysis (Table 2) shows that the crystallite sizes are almost the same in both powder and deposit specimens, and that the monoclinic zirconia is about an order-of-magnitude larger in size than the tetragonal zirconia. However, it should be noted that due to overlapping of different peaks, it was difficult to measure the FWHM of tetragonal peaks and, hence, the error in estimation of the tetragonal crystal size is expected to be large.

A TEM image of the zirconia powder is given in Fig. 9, and the particle size distribution, measured from this image, is presented in Fig. 10. These figures show that the specimen consists of spherical particles of size 7-18 nm. The specimen has a narrow size distribution with a mean particle size of about 12 nm. A few large sized (~ 40 nm) particles can also be seen in the micrograph, probably formed by the large sized droplets produced by the atomizer. SAD of these particles present a dominant ring structure, superimposed with some weak spots. It is believed that the rings are produced by the fine tetragonal zirconia particles, which is the dominant phase, while the weak spots are produced by the relatively larger sized (and strained) monoclinic zirconia particles.

3.3. Yttria stabilized zirconia (YSZ)

Figure 11 shows the microstructure of a typical specimen and indicates that the deposit is denser and more homogenous, as compared to the other specimens. In contrast to alumina and zirconia, which have distinct particulate structures, YSZ has a smoother surface texture. A high magnification image shows that the deposit consists of 20-100 nm particles. In some regions, these particles have bonded together to give a smooth surface.

XRD of typical specimens are presented in Fig. 12. Addition of the stabilizing agent (Y_2O_3) in the feedstock had no effect on phase structure. The XRD of the deposit is almost similar to that of the zirconia specimen (Fig. 8). However, the iron oxide phase is absent in this specimen, showing that the substrate had not been

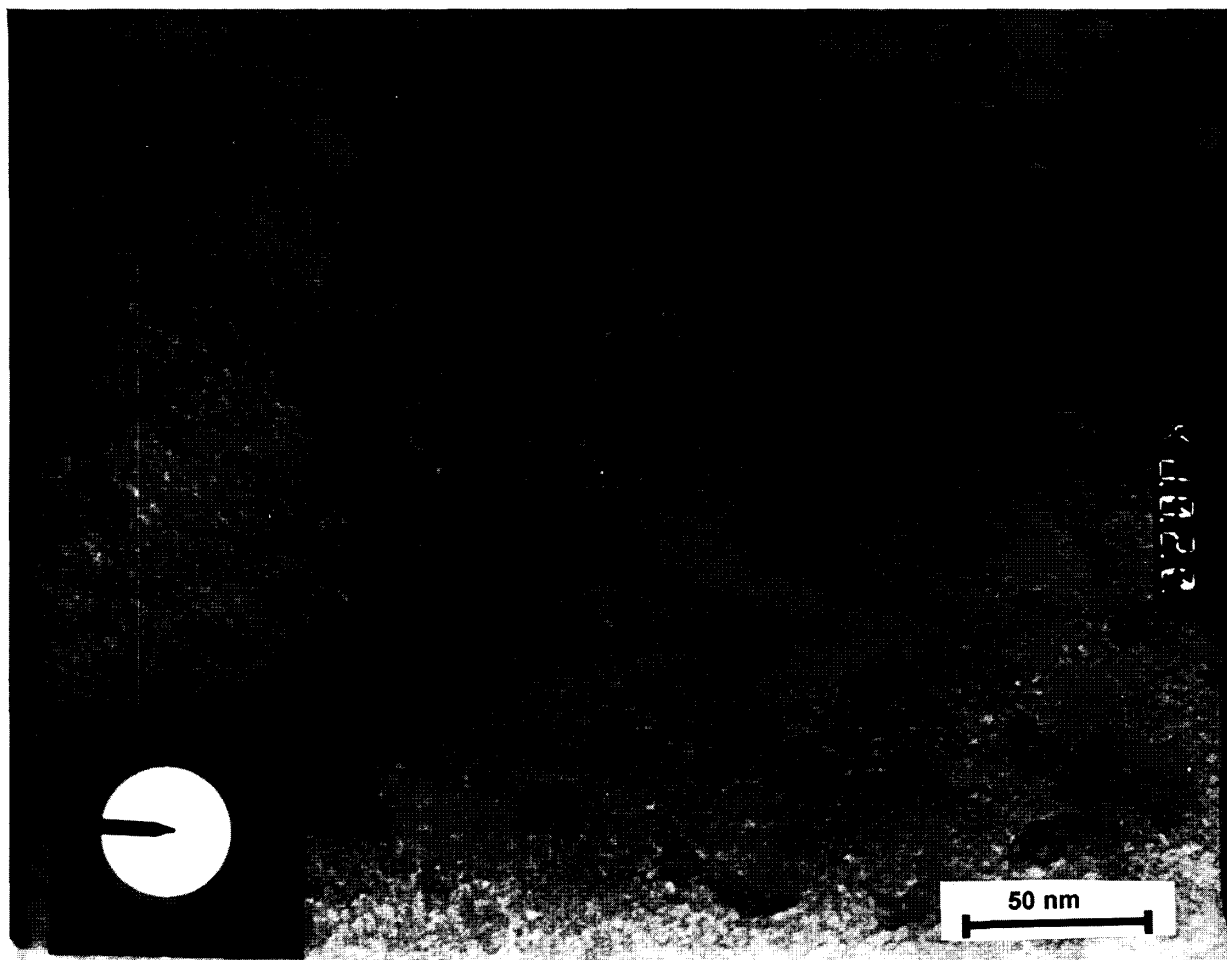


Fig. 6. Alumina powder collected in the electrostatic precipitator.

overheated during the spray process. The phase composition of the powder is exactly the same as that of zirconia; however, the diffraction peaks are much sharper in this specimen. The Scherrer analysis shows that the powder consists of larger sized monoclinic and smaller tetragonal zirconia particles. TEM studies show (Fig. 13) that this specimen contains relatively larger sized crystals than the alumina and zirconia specimens. Unlike zirconia, which contain spherical particles, the YSZ powder contains aggregates consisting of many nanoparticles. As Fig. 14 shows, these crystals have a wide size distribution in the range of 10–50 nm. Larger sized zirconia crystals of the specimen have given rise to distinct diffraction spots in SAD.

4. Discussion

The results have shown that the plasma spray synthesis (PSS) process can be used to produce nanostructured powders and deposits and that the specimen characteristics vary depending on the precursor and the

processing conditions. In the following section, a model of the PSS process is presented and the results discussed on the basis of the model.

In the plasma synthesis process, the liquid precursor is atomized and injected into the high temperature plasma flame, and the plasma synthesized particles are collected either as a deposit on a substrate or as powder on the electrostatic precipitator. As the atomized droplet enters the high temperature flame and is accelerated towards the collecting surface, various phenomena occur [9,23–26]. As shown in Fig. 15, the first step is the evaporation of the solvent, which is followed by condensation of the solid precursor materials. Chemical reactions are initiated next, and then nucleation and growth of the grains occur, resulting in the formation of dense particles. Interactions among these highly active particles lead to the formation of either 'large' particles/crystals, agglomerates or aggregates.

If the residence time of the droplets in the flame is short, as in the case when the collecting surface is placed at location A in Fig. 15, incomplete evaporation of the solvent and condensation of the precursor mate-

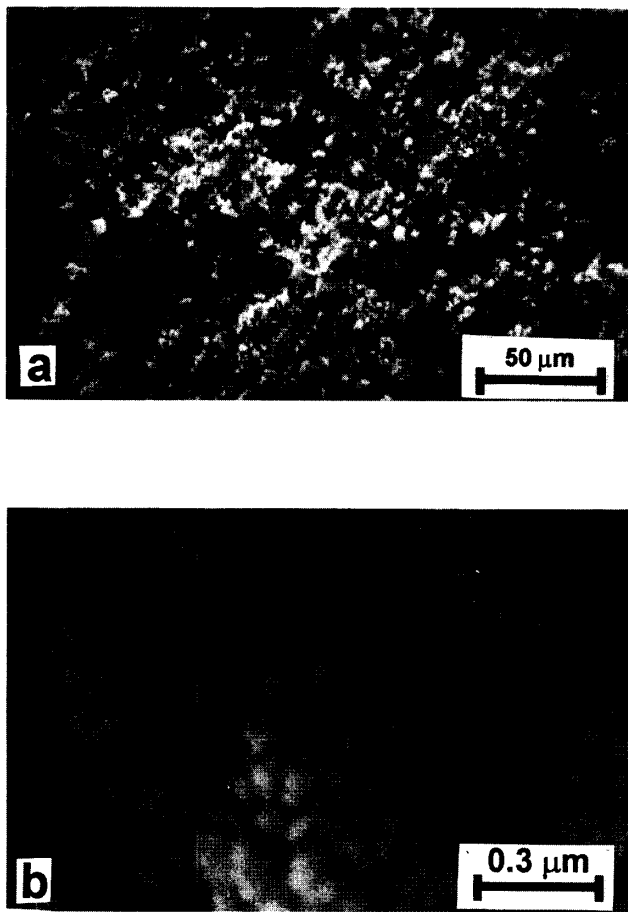


Fig. 7. SEM microstructures of a typical zirconia deposit at (a) low and (b) high magnifications.

rials occurs. This results in the liquid droplets splashing on the surface and then undergoing further reactions, depending on time and the availability of thermal energy. This leads to the formation of a patchy deposit.

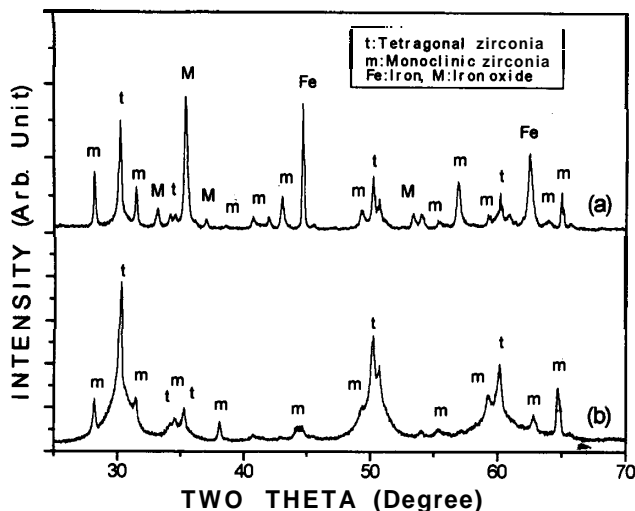


Fig. 8. XRD of zirconia specimens (a) deposit and (b) powder.

Chemical deposition is achieved at location B. Chemical reactions occur at or near the collecting surface at these locations, resulting in dense and adherent coatings. At location C, solid particles have already formed, but unlike a typical plasma spray process, they are not molten. Hence, a powdery deposit is obtained at this location.

As shown in Fig. 15, the collecting surface can be positioned at any of the locations, A, B and C. In practice, the stand-off distance of the collecting surface from the torch nozzle is varied. However, it should be noted that the physical, chemical and transport properties of the plasma, liquid droplet, solidified precursor and the synthesized particles strongly influence the precise location of A, B and C in the event chain shown in Fig. 15. Hence, the position of the locations vary depending on the experimental conditions.

The powder collection is more efficient at location C, while high quality deposits are obtained at position B. In this work, powder collection was carried out at location C, where we could obtain about 0.2 mg s^{-1} of nanomaterials. The rate of powder collection can be likely increased by increasing the size of the electrostatic precipitator and fine tuning the electrostatic precipitator, liquid atomizer injector and spray parameters.

Overheating and excessive oxidation of the substrate resulted when the stand-off distance was reduced to obtain specimens with strong and dense coatings, produced by reactants formed at or near the substrate (typically at location B). Oxidation of the substrate was observed even while obtaining powdery deposits at large stand-off distances. Hence, only powdery coatings were obtained in this study.

4.1. Alumina

The alumina deposit is powdery, indicating that the deposit has been formed by the deposition of solid particles at location C, as noted above. As expected, since the deposit is powdery, it has poor mechanical properties. The concentration of the alumina precursor solution was very low, only 1.5%. Moreover, even though the power level of operation was high, the liquid plasma spray process exhibited a deposition efficiency of $< 10.0\%$. Hence, preparation of typical deposits generally required long duration spray operation, which led to overheating and oxidation of the substrate even at a long stand-off distance, as shown by the XRD (Fig. 4).

Aluminum isopropoxide undergoes various phase changes when it is heated [27]. It is first converted to amorphous boehmite fibers and then is transformed to various alumina phases at different temperatures; i.e. γ at -800 K , δ at -1100 K , θ at -1300 K and α at -1400 K . The XRD studies (Fig. 5) indicate that the powder consists of low temperature γ alumina. When these γ

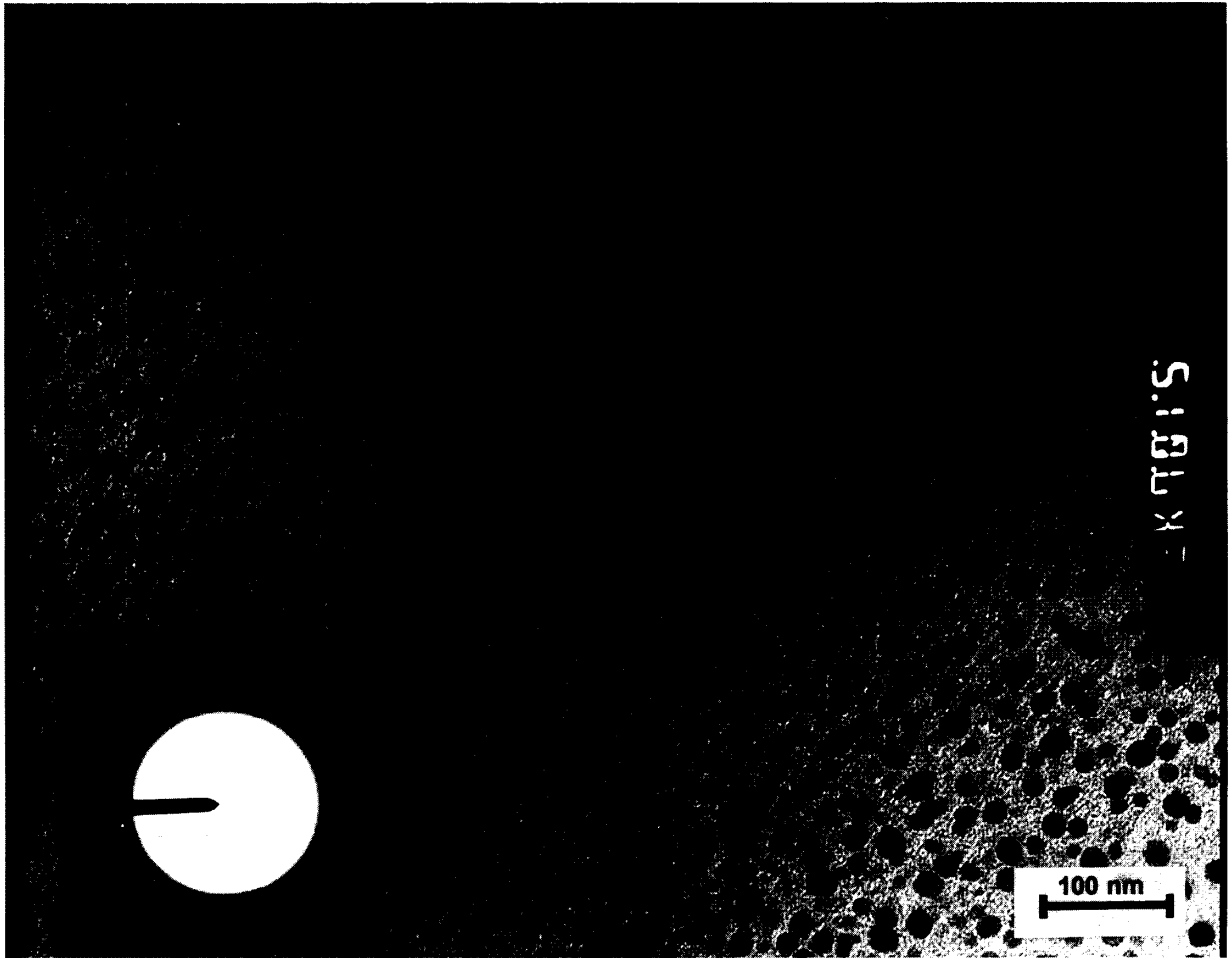


Fig. 9. TEM image of zirconia powder.

alumina particles deposit on the heated substrate surface, they are heated to > 1300 K and transform to θ alumina. Thermal activation of these particles on the

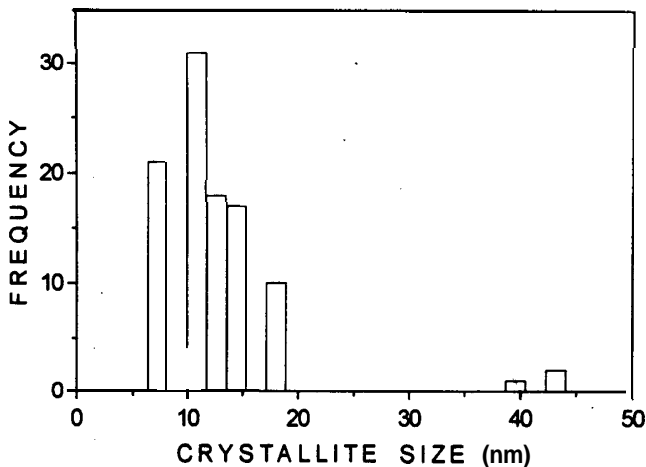


Fig. 10. Zirconia particle size distribution, measured from the TEM image (Fig. 9).

substrate also leads to the aggregation of the particles seen in Fig. 4b. As noted above, aluminum isopropoxide is first converted to amorphous fibers and then into γ alumina particles [28]. Nano-fibers transforming into nano-sized particles lead to the formation of rings and chains, which are visible in the TEM micrograph (Fig. 6). This micrograph is similar to the results reported by other investigators [10,28].

4.2. Zirconia

This specimen also presents a powdery structure. The microstructure is similar to the one reported by Chen and Mayo [29] for sintered zirconia, and shows that the deposit has been sintered during the deposition process. At room temperature, zirconia forms either a monoclinic or metastable tetragonal phase. The exact amount of metastable phase present in the specimen depends on the size and the thermal history of the particles or grains [30–32]. Skandan has shown that the weight fraction of the tetragonal zirconia present in nano-sized

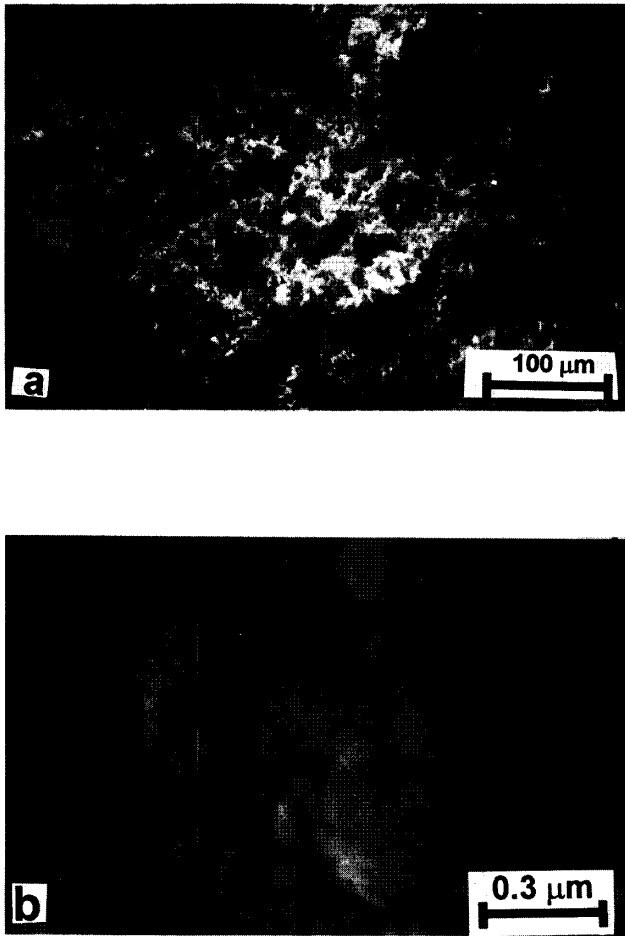


Fig. 11. Surface morphology of a typical YSZ specimen at (a) low and (b) high magnifications.

zirconia varies with the thermal history of the specimen [33]. Since the zirconia powder and deposit have undergone different thermal treatments during their manufacture, they contain different weight fractions of

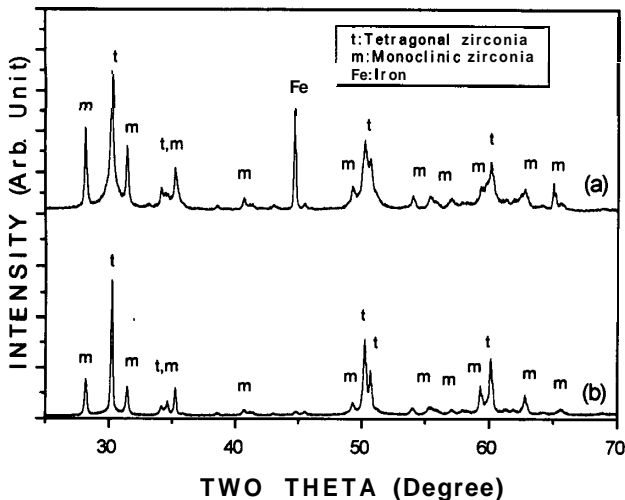


Fig. 12. XRD of YSZ specimens (a) deposit and (b) powder.

tetragonal zirconia. Similar TEM images of the spherical zirconia particle have been given by Lapatin et al. [34].

4.3. Ytria-stabilized zirconia

YSZ was prepared using an aqueous solution feedstock, while the alumina and zirconia feedstocks were prepared by dissolving the organo-metallic salts in alcohol. Injection of organic salt and alcohol into the plasma flame increases the heat content of the flame. This results in a long and intense flame and leads to heating and oxidation of the substrate material. Aqueous YSZ feedstock leads to a cooler flame and results in the formation of deposits free of iron oxide.

Vollath and Sickafus have found that the presence of water droplets or water vapor in the plasma reaction zone results in increasing the size and size range of the synthesized nanomaterials [12]. Since YSZ and zirconia specimens were produced with aqueous and metal-organic precursors respectively, formation of larger sized YSZ crystals as compared to zirconia particles can be understood. At present, it is not clear why the addition of the Y_2O_3 stabilizer had no effect on phase composition. Further work with different concentrations of stabilizer, heat treatment of the produced powder, and other experiments are required to elucidate this result.

5. Conclusions

Plasma Spray Synthesis, a new technique to produce nanomaterials has been developed. This technique uses an industrial plasma spray system to produce nanomaterials in open atmospheric air, and a simple parallel plate electrostatic precipitator to collect them. Nanomaterials, including alumina, zirconia and YSZ, have been produced by this process. The results of this study can be summarized as follows.

1. Nanoparticles and deposits were produced by injecting atomized liquid droplets of the precursor solution into plasma flame. Nanoparticles of zirconia, alumina and YSZ were produced in this work. Zirconia was produced as individual particles, while alumina and YSZ were formed as aggregates of nanoparticles.
2. Plasma spray synthesis is a single-step process. All of the reactions are driven to completion during the spray processing itself, resulting in the formation of nanosized ceramic grains or particles which are collected as a deposit or as powder. No post-spray calcination or heat treatment is required.
3. The size, shape and phase composition of the resulting nanomaterials depend strongly on the spray

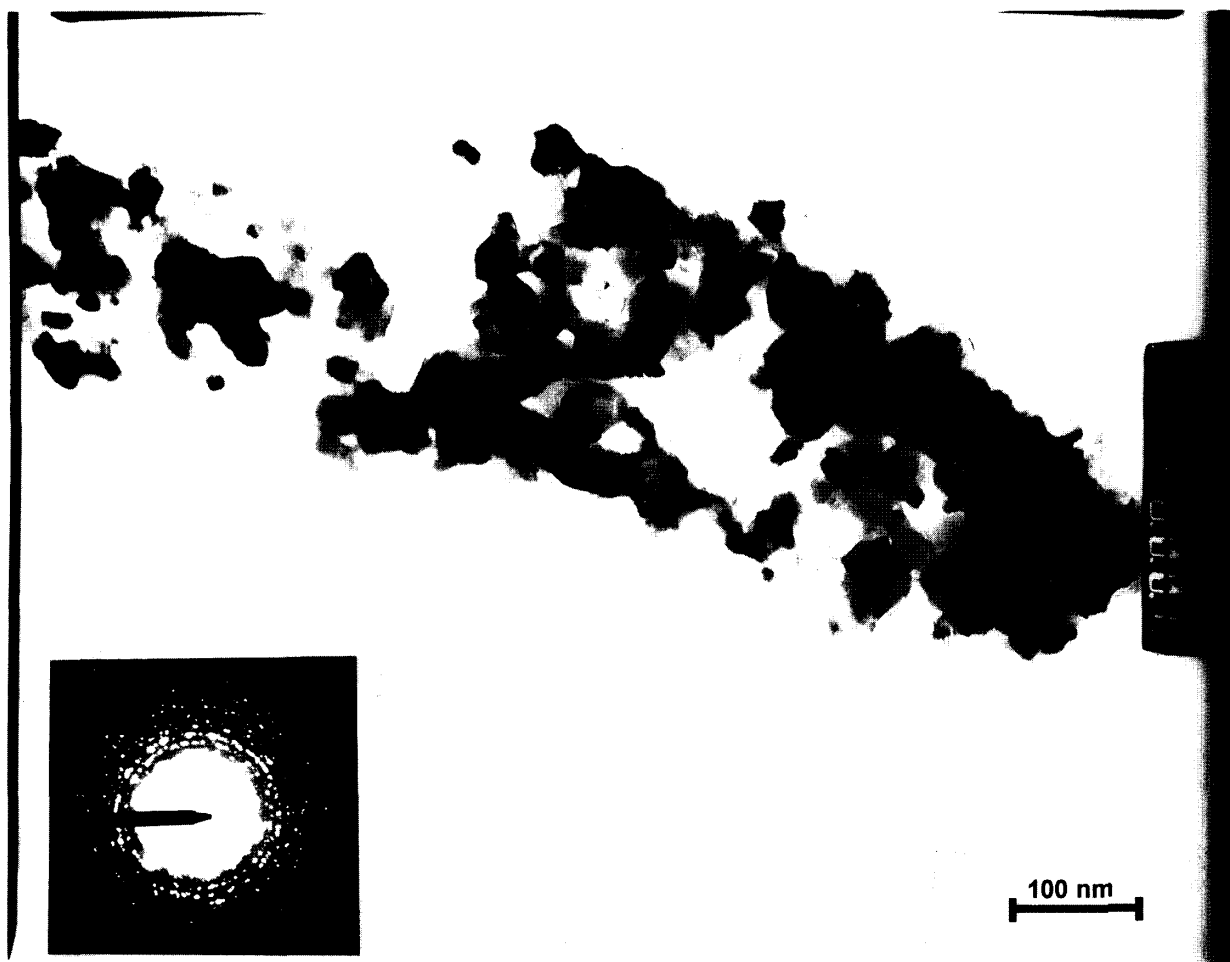


Fig. 13. TEM image showing the YSZ crystals.

feedstock. Aqueous solutions produced wider distributions of larger size grains, while organo-metallic solutions produced a narrow range of fine grained material.

4. Particles in the size range of 1–50 nm were collected at a rate of about 0.01 g min^{-1} , with about 20% collection efficiency. Further work is necessary to optimize the particle collection rate and the deposit characteristics.

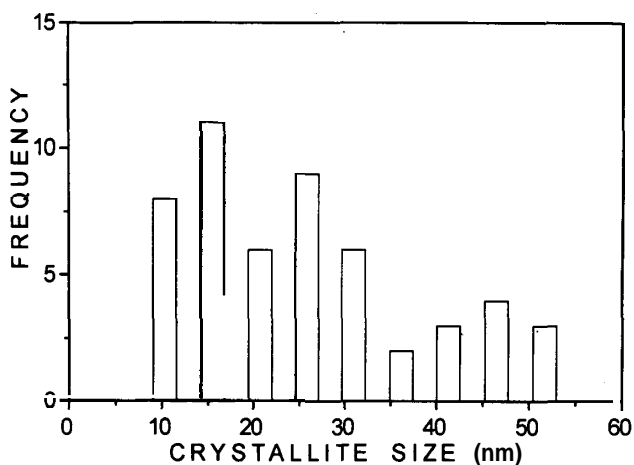


Fig. 14. Particle size distribution YSZ specimen, measured from the TEM image (Fig. 13).

Acknowledgements

This research program was sponsored by US National Science Foundation Grant # CTS- 931 2896. The authors would like to thank Prof. S. Sampath and Prof. A.H. King of Department of Materials Science and Engineering, SUNY at Stony Brook, Stony Brook, New York and Dr. J.R.T. Branco of Metallurgical Technology Department, Minas Gerais Technology Center Foundation-CETEC, Minas Gerais, Brazil, for many stimulating discussions and Ms. A. Ristorucci, Dr. J.Y. Wang, and Dr. J. Quinn of Department of Materials Science and Engineering, SUNY at Stony Brook, Stony Brook, New York for experimental assistance.

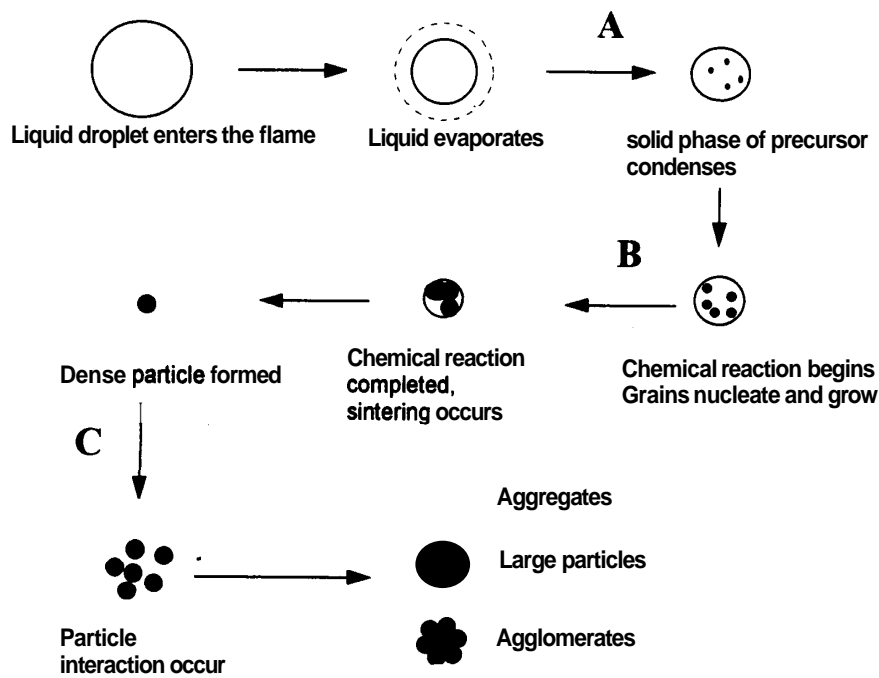


Fig. 15. Schematic of the Plasma Spray Synthesis process Refer to the text for A, B and C.

References

- [1] H. Gleiter, Nanocrystalline Materials, *Prog. Mater. Sci.* 33 (4) (1990) 223–315.
- [2] M. Gell, Application opportunities for nanostructured materials and coatings, *Mater. Sci. Eng. A204* (1-2) (1995) 246–251.
- [3] R.W. Siegel, Nanostructured materials—mind over matter, *Nanostruct. Mater.* 3 (1) (1993) 1–18.
- [4] C.C. Koch, The synthesis and structure of nanocrystalline materials produced by mechanical attrition: a Review, *Nanostruct. Mater.* 2 (2) (1993) 109–129.
- [5] R. Uyeda, Studies of ultrafine particles in Japan: crystallography, methods of preparation and technological application, *Prog. Mater. Sci.* 35 (1) (1991) 1–96.
- [6] B.H. Kear, L.E. Keem, R.W. Siegel, F. Spaepen, K.C. Taylor, E.L. Thomas, K.N. Tu, *Research Opportunities for Materials with Ultrafine Microstructures* vol. NMAB-454, National Academy, Washington, DC, 1989.
- [7] H. Gleiter, Materials with ultrafine microstructures; retrospectives and perspectives, *Nanostruct. Mater.* 1 (1) (1992) 1–20.
- [8] G.F. Gaertner, P.F. Miquel, Particle generation by laser ablation from solid targets in gas flows, *Nanostruct. Mater.* 4 (3) (1993) 559–568.
- [9] J.L. Katz, P.F. Miquel, Synthesis and applications of oxides and mixed oxides produced by a flame process, *Nanostruct. Mater.* 4 (5) (1994) 551–557.
- [10] B. Gunther, A. Kumpmann, Ultrafine oxide powders prepared by inert gas evaporation, *Nanostruct. Mater.* 1 (1) (1992) 27–30.
- [11] Y. Mizoguchi, M. Kagawa, M. Suzuki, Y. Syono, T. Hirai, Synthesis of ultrafine particles and thin films of $\text{BaFe}_{12}\text{O}_{19}$ by spray ICP technique, *Nanostruct. Mater.* 4 (5) (1994) 591–596.
- [12] D. Vollath, K.E. Sickafus, Synthesis of nanosized ceramic oxide powders by microwave plasma reactions, *Nanostruct. Mater.* 1 (5) (1992) 427–437.
- [13] A.E. Petrov, A.P. Orlov, Ya.K. Vaivads, S.V. Belogurov, A.A. Kuzuyevich, Plasmachemical treatment of ferrite powders and their magnetic properties in high dispersive state, *Sov. Pow. Met. Met. Ceram.* 30 (6) (1991) 445–447.
- [14] C.J. Brinker, G.W. Scherer, *Sol-Gel Science: The Physics and Chemistry of Sol-Gel Processing*, Academic Press, San Diego, CA, 1990.
- [15] R. Suryanarayanan, *Plasma Spraying: Theory and Applications*, World Scientific, Singapore, 1993.
- [16] P.G. Tsanztrizos, The reaction spray forming production of titanium aluminide in the tail flame of a DC plasma torch, in: C.C. Berndt (Ed.), *Thermal Spray: International Advances in Coating Technology*, ASM, OH, 1992, pp. 195–199.
- [17] N. Ohtake, M. Yoshikawa, Diamond film preparation by arc discharge plasma jet chemical vapor deposition in the methane atmosphere, *J. Electrochem. Soc.* 2 (3) (1990) 717–722.
- [18] O.M. Grebtsova, E.P. Domashneva, E.N. Kurtin, A.A. Budanov, Plasma chemical synthesis of oxides in Y–Ba–Cu–O system, *Sov. Pow. Met. Met. Ceram.* 31 (10) (1992) 822–825.
- [20] H.P. Klug, L.E. Alexander, *X-ray Diffraction Procedure for Polycrystalline and Amorphous Materials*, 2nd edn., Wiley, New York, 1974.
- [21] T. Ekstrom, C. Chatfield, W. Wruess, M.M. Schreiber, The use of X-ray diffraction peak broadening to characterize ground Al_2O_3 powders, *J. Mater. Sci.* 20 (4) (1985) 1266–1274.
- [22] S.K. Pradhan, T. Chakraborty, S.P. Sen Gupta, C. Suryanarayana, A. Frefer, F.H. Froes, X-ray powder profile analysis on nanostructured niobium metal powders, *Nanostruct. Mater.* 5 (1) (1995) 53–61.
- [23] A. Gurav, T. Kodas, T. Pluym, Y. Xiong, Aerosol processing of materials, *Aerosol Sci. Technol.* 19 (1993) 411–452.
- [24] C. Roger, T. Corbitt, C. Xu, D. Zeng, Q. Powell, M. Nyman, M.J. Hampden-Smith, T. T. Kodas, Principles of molecular precursor selection for aerosol synthesis of materials, *Nanostruct. Mater.* 4 (5) (1994) 529–535.
- [25] S.K. Friedlander, R.S. Windeler, A.P. Weber, Ultrafine particles formation in turbulent jets: mechanisms and scale-up, *Nanostruct. Mater.* 4 (5) (1994) 521–528.

- [26] I. Wiedemann, K.L. Choy, B. Derby, Flame-assisted deposition of lead titanate-based thin films; correlation of deposition process, microstructure and electrical properties, in: F.R. Sale (Ed.), *Novel Synthesis and Processing of Ceramics*. The Institute of Materials, London, 1994, pp. 133–142.
- [27] W.H. Gitzen (Ed.), *Alumina as a Ceramic Material*, The American Ceramic Society, OH, 1970, p. 17.
- [28] C.M. Wang, F.L. Riley, Morphological changes during the calcination of oxide-coated silicon nitride powder, in: F.R. Sale (Ed.), *Novel Synthesis and Processing of Ceramics*, The Institute of Materials, London, 1994 pp. 235–248.
- [29] D.J. Chen, M.J. Mayo, Densification and grain growth of ultrafine 3 mol% Y_2O_3 - ZrO_2 ceramics, *Nanostruct. Mater.* 2 (5) (1993) 469–478.
- [30] R.C. Garvie, R.H. Hannink, R.T. Poscoe, Ceramic steel?, *Nature* 258 (1975) 703–704.
- [31] R.C. Garvie, M.V. Swain, Thermodynamic analysis of the tetragonal to monoclinic transformation in a constrained zirconia microcrystal. Part I, *J. Mater. Sci.* 20 (4) (1985) 1193–1200.
- [32] C.A. Anderson, P.K. Gupta, Phase stability and transformation toughening in zirconia, in: A.H. Heuer, L.W. Hobbs (Eds.), *Adv. in Ceramics, vol. 3: Science and Technology of Zirconia*, The American Ceramic Society, OH, 1981, pp. 184–201.
- [33] G. Skandan, Processing of nanostructured zirconia ceramics, *Nanostruct. Mater.* 5 (2) (1995) 111–126.
- [34] V.V. Lapatin, U.F. Ivanov, V.S. Dedkov, Structure-diffraction analysis of nanometer-sized polycrystals, *Nanostruct. Mater.* 4 (6) (1994) 669–676.